Stabilization and Observation of Large-area Ferromagnetic Bimeron Lattice

Miming Cai,[1,2,*] Shangyuan Wang,[1,2,*] Yuelin Zhang,[1,2,*] Xiaoqing Bao,[1,2] Dekun Shen,[1,2] Jinghua Ren,[1,2] Lei Qiu[1,2], Haiming Yu[3], Zhenlin Luo[4], Mathias Kläui[5], Shilei Zhang[6], Nicolas Jaouen[7], Gerrit van der Laan[8], Thorsten Hesjedal[9], Ka Shen[1,2,10,†] and Jinxing Zhang[1,2,†]

[1]*School of Physics and Astronomy, Beijing Normal University, Beijing 100875, China.*

[2]*Key Laboratory of Multiscale Spin Physics, Ministry of Education, Beijing 100875, China.*

[3]*Fert Beijing Institute, MIIT Key Laboratory of Spintronics, School of Integrated Circuit Science and Engineering, Beihang University, Beijing 100191, China*

[4]*National Synchrotron Radiation Laboratory, University of Science and Technology of China, Hefei 230026, China.*

[5]*Institute of Physics, Johannes Gutenberg University Mainz, Staudinger Weg 7, Mainz 55128, Germany*

[6]*School of Physical Science and Technology, ShanghaiTech University, Shanghai 200031, China*

[7]*Synchrotron SOLEIL, L'Orme des Merisiers, 91192 Gif-sur-Yvette, France.*

[8]*Diamond Light Source, Harwell Science and Innovation Campus, Didcot OX11 0DE, UK.*

[9]*Department of Physics, University of Oxford, Oxford OX1 3PU, UK.*

[10]*The Center for Advanced Quantum Studies, Beijing Normal University, Beijing 100875, China*

*These authors contributed equally to this work.

†Correspondence to: kashen@bnu.edu.cn; jxzhang@bnu.edu.cn

Abstract

Symmetry engineering is an effective approach for generating emergent phases and quantum phenomena. In magnetic systems, the Dzyaloshinskii-Moriya (DM) interaction is essential for stabilizing chiral spin textures. The symmetry manipulation of DM vectors, described in three dimensions, could provide a strategy towards creating abundant topologically magnetic phases. Here, we have achieved to break the rotational and mirror symmetries of the three-dimensional DM vectors in a strongly correlated ferromagnet, which were directly measured through the nonreciprocal spin-wave propagations in both in-plane and out-of-plane magnetic field geometries. Combining cryogenic magnetic force microscopy and micromagnetic simulations, we discover a bimeron phase that emerges between spin spiral and skyrmion phases under an applied magnetic field. Such an artificially manipulated DM interaction is shown to play a critical role in the formation and evolution of the large-area bimeron lattice, a phenomenon that could be realized across a broad range of materials. Our findings demonstrate that symmetry engineering of the DM vectors can be practically achieved through epitaxial strain, paving the way for the creation of diverse spin topologies and the exploration of their emergent functionalities.

Exploration of topological spin textures in real space provides a platform to study the fundamental structures and emergent phenomena of solitons in physics [1-3], and offers potential applications as ideal information units for beyond-CMOS logic and storage devices [4-6]. This has drawn significant attention from researchers across physics, materials science, and information technology [7-9]. Among these spin textures, magnetic skyrmions are particularly notable [10,11], with their stabilization governed by the Dzyaloshinskii-Moriya interaction (DMI) alongside the interplay of magnetocrystalline anisotropy, Zeeman energy, and magnetostatic energy. Since the discovery of DMI in ferromagnetic materials, systems that majorly exhibit interfacial-like [12,13] and bulk-like DMI [13-15] have been observed, which results in the formation of Néel-type and Bloch-type skyrmions as shown in Fig. 1(a) and 1(b), as well as merons [16-24], hopfions [25-27], chiral bobbers [28,29] and skyrmion strings[30,31], to name a few.

In physics, emergent phases or phenomena often arise when symmetry is reduced or broken [32]. In ferromagnets with DMI, the DM vectors can be described in the *x*-, *y*-, and *z*-directions of a three-dimensional Cartesian coordinate system [33], which allows the use of the elements and operations of crystal symmetry elements and operations to describe the symmetry of the DMI [34,35]. In the majority of cases, the DM vectors generating the topological spin textures [9,10,14-29] adhere to a relatively high degree of symmetry. A natural question arises: can reducing or breaking the symmetry of the DM vectors create opportunities for novel topological variants in

magnets? In 2006, Bogdanov *et al.* predicted that lower symmetry of DM vectors may bring about more non-trivial spin configurations [34]. Recent experiments have further suggested that reducing DM vectors symmetry (i.e., anisotropic DMI) may stabilize exotic spin textures such as antiskyrmions [36-38]. Theoretical studies reveal that DM vectors without rotational and mirror symmetries could give rise to the emergent topological magnetic textures such as bimeron [Fig. 1(c)], which may possess extraordinary dynamic properties under excitation compared to classical skyrmions [33,39]. Therefore, manipulating the symmetry of DM vectors may open the door to a richer variety of spin topologies, as summarized in Fig. S1 and Table SI (Supplementary Information Section S2 [40]).

Despite the theoretical interests in stabilizing topological variants such as bimeron lattices through controllable DM vectors symmetry in three dimensions, experimental realization still remains a challenge. Recently, Zhang *et al.* demonstrated that graded strain can effectively break the spatial inversion symmetry of crystals [47], creating a hybrid DMI in three dimensions and offers the possibility of engineering the desired symmetry of DM vectors. In this study, we show that DM vectors without rotational (C_n) and mirror (σ) symmetries can be artificially designed in a ferromagnetic oxide thin film, (La,Sr)MnO_3 (LSMO). Such a DMI are formed by the flexoresponse of the magnetic order with the strain gradient [48]. We directly observe the formation and evolution of a large-area bimeron lattice under varying external magnetic field, tracking its emergence from a spin spiral to a skyrmion lattice.

The DM vectors of magnetic materials can be described by the following tensor (1) [47]

$$\boldsymbol{D} = \begin{bmatrix} \boldsymbol{D}_x \\ \boldsymbol{D}_y \\ \boldsymbol{D}_z \end{bmatrix} = \begin{bmatrix} D_{xx} & D_{xy} & D_{xz} \\ D_{yx} & D_{yy} & D_{yz} \\ D_{zx} & D_{zy} & D_{zz} \end{bmatrix} \quad (1)$$

where D_{ij} with $i = x, y, z$ represents the jth component of the DM vector for the spin pairs along [100], [010], and [001] axes, respectively. In the case of non-uniform strain, $D_{ij} = \nu_{ijmlk} E_{ml,k}$ where ν_{ijmlk} are the corresponding flexo-responsive coefficients of the strain-gradient components $E_{ml,k}$. Apart from the conventional DM components in the interfacial-like and bulk-like DMI ($D_{xx},\ D_{yy},\ D_{zz},\ D_{xy},\ D_{yx}$), the existence of z-components ($D_{xz},\ D_{yz},\ D_{zx},\ D_{zy}$) is essential for achieving control over the symmetry of DM vectors in three dimensions. This motivates experimental exploration of DM components' configuration in the LSMO films and deterministic control of DM vectors symmetry via epitaxial strain modulation. For this purpose, a high-quality LSMO film with a strain relaxation and thickness of ~150 nm was epitaxially grown on $NdGaO_3$ substrate (Supplementary Information Section S3, Figs. S2 and S3 [40]).

The nonreciprocity of spin-wave propagation is usually used to identify the existence and amplitude of DMI [49-53]. To evaluate DM components in strain-graded LSMO film, spin-wave propagation in a fully in-plane and out-of-plane magnetized LSMO film was characterized using a vector network analyzer in combination with a microwave probe (Supplementary Information Section S1 and S4 [40]). The detailed geometries for measuring the in-plane (D_{yx}) and out-of-plane (D_{xz}) components are

illustrated in Figs. 2 and S4 [40]. For the former, the propagating spin wave along the *y*-axis was measured under magnetic saturation along the *x*-axis (also called Damon-Eshbach, DE mode). With an applied in-plane field of $\mu_0 H_{\mathrm{ext}}$ = 140 mT [Fig. 2(a)], frequency nonreciprocity of $\delta f_{yx}(k) = f_{\mathrm{DE}}(+k) - f_{\mathrm{DE}}(-k) \approx -0.06$ GHz (**H** ∥ x) is observed [Fig. 2(c)], which is proportional to D_{yx} according to

$$f_{\mathrm{DE}}(\pm k, H_{\mathrm{ext}}) = \frac{\gamma\mu_0}{2\pi}\sqrt{(Jk^2 - \xi + H_{\mathrm{ext}} + M_{\mathrm{s}})(Jk^2 + \xi + H_{\mathrm{ext}})} \mp \frac{\gamma k}{\pi M_{\mathrm{s}}} D_{\mathrm{yx}} \qquad (2)$$

where $J = 2A/\mu_0 M_{\mathrm{s}}$ and $\xi = M_{\mathrm{s}}\left(1 - e^{-2|k|d}\right)/4$ with A being the exchange constant, M_{s} the saturation magnetization, μ_0 the vacuum permeability, γ the gyromagnetic ratio, d the thickness, k the wave vector, and H_{ext} the external field. The value of the in-plane DM component $D_{yx} = 1.41\times10^{-4}$ J m^{-2} is estimated by using the material parameters and $k = 2.07$ rad μm^{-1}.

Furthermore, the out-of-plane DM component D_{xz} can also lead to a frequency nonreciprocity in the magnetostatic forward volume (FV) spin waves. Therefore, we extend our non-local measurement to the FV modes. To the best of our knowledge, this has remained unexplored due to the absence of materials systems that exhibit an out-of-plane D_{xz} component. Our experimental setup including an axially rotatable electromagnet provides a magnetic vector field. The propagating spin wave along the *x*-axis is measured under magnetic saturation along the *z*-axis in an out-of-plane magnetic field [Fig. 2(b)]. During the measurement, the external magnetic field $\mu_0 H_{\mathrm{ext}}$ = 550 mT is applied along the *z*-axis for magnetic saturation. The magnetic hysteresis loop can be found in Fig. S3. A frequency nonreciprocity $\delta f_{xz} = f_{\mathrm{FV}}(+k) -$

$f_{\mathrm{FV}}(-k) \approx 0.04$ GHz is observed [Fig. 2(d)]. The D_{xz} component is estimated though [54]

$$f_{\mathrm{FV}}(\pm k, H_{\mathrm{ext}}) = \frac{\gamma\mu_0}{2\pi}\sqrt{(Jk^2 + \zeta + H_{\mathrm{ext}} + M_{\mathrm{eff}})(Jk^2 + H_{\mathrm{ext}} + M_{\mathrm{eff}})} \mp \frac{\gamma k}{\pi M_{\mathrm{s}}} D_{\mathrm{xz}} \quad (3)$$

where $\zeta = M_{\mathrm{s}}[1 - (1 - e^{-kd})/kd]$, $M_{\mathrm{eff}} = \mu_0 H_{\mathrm{ani}} - \mu_0 M_{\mathrm{s}}$, and $\mu_0 H_{\mathrm{ani}}$ is the perpendicular anisotropy field. $D_{xz} = -0.94\times10^{-4}$ J m^{-2} is estimated for the out-of-plane DM component. The spin-wave dispersion of FV modes was further simulated, as shown in Fig. S5, which confirms that this frequency nonreciprocity originates from the D_{xz} components. More details of the exploration of additional DM components can be found in Fig. S6 [40]. The comparable values of the in-plane and out-of-plane DM components clearly reveal a symmetry configuration of DM vectors in the LSMO film, e.g. a breaking of rotational (C_{n}) and mirror (σ) symmetries of the DM vectors as illustrated in Fig. 1(c) [33]. Such a DM configuration therefore provides an ideal platform for stabilizing more emergent topological magnetic textures.

To investigate the possible existence and evolutions of emergent topological magnetic phases in real space, we employed cryogenic magnetic force microscopy (MFM) to image the magnetic domains under varying external fields (Supplementary Information Section S1 [40]). At 3.6 K, a spin spiral state, confirmed by sinusoidal profile of the MFM phase [Fig. S8] [55], was observed without magnetic field, as shown in the top panel of Fig. 3(a). The intensity of the MFM signal along the dashed path is plotted in the bottom panel. It shows the same spiral characteristic as observed at room temperature, exhibiting an excellent periodicity over a large area. This periodicity has

been characterized by MFM and resonant elastic x-ray scattering (REXS) [Fig. S7]. When a magnetic field over -0.12 T was applied perpendicular to the film surface, the decreasing MFM contrast intensity suggested a reduction of the local out-of-plane magnetization and an appearance of an "intermediate" spiral state [Fig. S9]. At a magnetic field of -0.3 T, the "intermediate" spin spiral phase forms completely [Fig. 3(b)]. Both spiral states share a similar periodicity as confirmed by Fast Fourier Transform (FFT) analysis [insets of Fig. 3(a) and 3(b)].

When the applied field strength exceeds -0.4 T, an unexpected magnetic phase emerges, characterized by pairs of semicircles with reversed out-of-plane magnetization cores, forming as a triangular arrangement [Fig. 3(c)]. Further increasing the external magnetic field strength to -0.465 T results in a transition to the skyrmion phase [Fig. 3(d)]. Notably, the FFT pattern of this emergent magnetic phase displays a distorted hexagonal periodicity, corresponding the arrangement in real space, as shown in the top panel of Fig. 3(c). It is distinct from the symmetric hexagonal periodicity characteristic of the skyrmion phase [insets of Fig. 3(c) and 3(d)]. This lattice of paired semicircles, exhibiting a periodic arrangement, is an emergent phase rarely observed in magnets with traditional DMI [11,56]. The detailed evolution from the bi-core lattice state to skyrmion lattice is presented in Fig. S10 [40].

Micromagnetic simulations using MUMAX3 [57] were conducted to better understand the nature and origin of the emergent magnetic phase with reversed cores

and associated chirality, assuming the DM vectors with both out-of-plane and in-plane components like Fig. 1(c) [33]. The adopted parameters can be found in the Supplementary Information Section S1 [40]. As plotted in Fig. 4, all the experimentally observed phases are reproduced. The comparison between simulated results in Fig. 4(a) and 4(b) suggests that the transition of the spiral states as observed in Fig. 3(a) and 3(b) corresponds to the relative shrinking of two up/down magnetized domains under the perpendicular magnetic field. For the emergent phase with paired semicircles, the magnetization distribution of each bi-core unit matches that of the predicted ferromagnetic bimeron [33]. The ferromagnetic bimeron lattice evolves into the magnetic skyrmion phase at increased magnetic fields. The number of bimerons is equal to that of skyrmions, indicating the one-by-one transformation between these two topological spin textures [Fig. 4(c) and 4(d)]. The spin configuration at the top layer is shown in Fig. 4(a)-(d) bottom panel. Those at the middle and bottom layers are shown in Fig. S11. Each layer retains the bimeron configuration with slightly differences in size [Fig. S11(c)] due to the demagnetizing field [58]. Figure 4(f) reveals the combination of two specific chirality along the *x*- and *y*-axes in a bimeron [Fig. 4(e)], induced by the in-plane and out-of-plane DM components, i.e., D_{yx} and D_{xz}, respectively.

It is also noteworthy that, simulations with only interfacial DMI or without any DMI cannot be the case in the present observation, as shown in Fig. S12. Therefore, we conclude that the bimeron phase are driven by the three-dimensional DM vectors. This

symmetry engineering of DM vectors facilitates the large-area stabilization of the bimeron lattice observed experimentally [Fig. S13]. The temperature-magnetic-field phase diagram [Fig. S14], capturing intermediate states, provides critical insights into this transition and fills a previously unexplored gap of the bimeron phase between spiral and skyrmion states. Our findings propose a practical strategy for tailoring magnetic textures by designing and controlling symmetry of DM vectors. Graded strain offers a precise method for engineering them via the interplay of crystal structure and the strain configuration [47,48], such as the relaxation of shear strain or anisotropic biaxial strain, which may independently break the symmetry of the DM vectors and generate further variants of magnetic textures. This approach may extend beyond bimerons and skyrmions to a broader spectrum of magnetic phases, enabling the on-demand design of topological magnetic textures.

Conclusions

In summary, a three-dimensional DM configuration breaking rotational and mirror symmetries, was artificially designed in a strain-graded LSMO thin film and quantitatively characterized by nonreciprocal spin-wave propagation. Such a DM configuration facilitated the stabilization of a large-area ferromagnetic bimeron lattice, which was directly observed during the phase evolution from a spin spiral to skyrmion state. Micromagnetic simulations highlighted the crucial role of the DM configuration with both out-of-plane and in-plane DM components in shaping this emergent

topological spin texture. Our results demonstrate that artificially designed symmetry of DM vectors and its associated topological variants can be extended to a wide range of materials. The large-area bimeron phase observed in this strongly correlated oxide provides a novel platform for exploring emergent functionalities and quantum phenomena in both ground and excited states.

Acknowledgements

This work was supported by the National Natural Science Foundation (NSFC) of China (grant no. 52225205, J.Z.), the National Key Research and Development Program of China (grant no. 2023YFA1406500, J.Z. and grant no. 2021YFA0718700, J.Z.) and the Fundamental Research Funds for the Central Universities (J.Z., K.S. and Y.Z.). We also acknowledge the support of the NSFC (grants nos. T2350005, J.Z.; 11974047, K.S.; 12374100, K.S.; 12404119, Y.Z.), the Beijing Natural Science Foundation (Z240008, J.Z.) and the National Key R&D Program of China (grant no. 2022YFA1402801, H.Y.). The group in Mainz acknowledges support by the Deutsche Forschungsgemeinschaft (DFG, German Research Foundation) projects 403502522 (SPP 2137 Skyrmionics), 49741853, and 268565370 (SFB TRR173 projects A01, B02 and A12) as well as TopDyn. The work is a highly interactive collaboration supported by the Horizon 2020 Framework Program of the European Commission under ERC-2019-SyG no. 856538 (3D MAGiC) and the Horizon Europe project no. 101070290 (NIMFEIA).

Author contributions

M.C., Y.Z. and J.Z. conceived and designed the experiments. D.S. and J.R. were responsible for the thin film fabrication. M.C., Z.L., performed structural and magnetic characterization. M.C. and X.B. performed magnetic force microscopy. M.C., D.S., Y.Z. and H.Y. designed and fabricated the CPWs and performed the spin-wave propagation measurements. S.W., L.Q. and K.S. performed the micromagnetic simulation. S.Z., M.K. and N.J. were responsible for the designs or measurements of resonant elastic x-ray scattering. J.Z. supervised the experimental study, and H.Y., M.K., N.J., G.L. and T.H. provided related discussion. K.S. supervised the theoretical and simulated study. M.C., S.W., Y.Z., K.S. and J.Z. wrote the paper. M.K., S.Z., N.J., G.L. and T.H. contributed to the revision.

References

[1] L. Brey, H. A. Fertig, R. Côté, and A. H. MacDonald, Phys. Rev. Lett. **75**, 2562 (1995).

[2] U. Al Khawaja and H. Stoof, Nature **411**, 918 (2001).

[3] A. N. Bogdanov, U. K. Rößler, M. Wolf, and K. H. Müller, Phys. Rev. B **66**, 214410 (2002).

[4] J. Iwasaki, M. Mochizuki, and N. Nagaosa, Nat. Nanotechnol. **8**, 742 (2013).

[5] W. Jiang, P. Upadhyaya, W. Zhang, G. Yu, M. B. Jungfleisch, F. Y. Fradin, J. E. Pearson, Y. Tserkovnyak, K. L. Wang, O. Heinonen, S. G. te Velthuis, and A. Hoffmann, Science **349**, 283 (2015).

[6] O. Lee, R. Msiska, M. A. Brems, M. Kläui, H. Kurebayashi, and K. Everschor-Sitte, Appl. Phys. Lett. **122**, 260501 (2023).

[7] A. Fert, N. Reyren, and V. Cros, Nat. Rev. Mater. **2**, 17031 (2017).

[8] C. Back, V. Cros, H. Ebert, K. Everschor-Sitte, A. Fert, M. Garst, T. Ma, S. Mankovsky, T. L. Monchesky, M. Mostovoy, N. Nagaosa, S. S. P. Parkin, C. Pfleiderer, N. Reyren, A. Rosch, Y. Taguchi, Y. Tokura, K. von Bergmann, and J. Zang, J. Phys. D: Appl. Phys. **53**, 363001 (2020).

[9] B. Göbel, I. Mertig, and O. A. Tretiakov, Phys. Rep. **895**, 1 (2021).

[10] S. Mühlbauer, B. Binz, F. Jonietz, C. Pfleiderer, A. Rosch, A. Neubauer, R. Georgii, and P. Böni, Science **323**, 915 (2009).

[11] X. Z. Yu, Y. Onose, N. Kanazawa, J. H. Park, J. H. Han, Y. Matsui, N. Nagaosa, and Y. Tokura, Nature **465**, 901 (2010).

[12] P. M. Levy and A. Fert, Phys. Rev. B **23**, 4667 (1981).

[13] A. R. Fert, Mater. Sci. Forum **59-60**, 439 (1991).

[14] A. Bogdanov and A. Hubert, J. Magn. Magn. Mater. **138**, 255 (1994).

[15] S. Seki, X. Z. Yu, S. Ishiwata, and Y. Tokura, Science **336**, 198 (2012).

[16] T. Shinjo, T. Okuno, R. Hassdorf, K. Shigeto, and T. Ono, Science **289**, 930 (2000).

[17] R. Hertel, S. Gliga, M. Fähnle, and C. M. Schneider, Phys. Rev. Lett. **98**, 117201 (2007).

[18] M. Curcic, B. Van Waeyenberge, A. Vansteenkiste, M. Weigand, V. Sackmann, H. Stoll, M. Fahnle, T. Tyliszczak, G. Woltersdorf, C. H. Back, and G. Schutz, Phys. Rev. Lett. **101**, 197204 (2008).

[19] C. Phatak, A. K. Petford-Long, and O. Heinonen, Phys. Rev. Lett. **108**, 067205 (2012).

[20] S. Wintz, C. Bunce, A. Neudert, M. Korner, T. Strache, M. Buhl, A. Erbe, S. Gemming, J. Raabe, C. Quitmann, and J. Fassbender, Phys. Rev. Lett. **110**, 177201 (2013).

[21] S.-Z. Lin, A. Saxena, and C. D. Batista, Phys. Rev. B **91**, 224407 (2015).

[22] A. Nych, J.-i. Fukuda, U. Ognysta, S. Žumer, and I. Muševič, Nat. Phys. **13**, 1215 (2017).

[23] X. Z. Yu, W. Koshibae, Y. Tokunaga, K. Shibata, Y. Taguchi, N. Nagaosa, and Y. Tokura, Nature **564**, 95 (2018).

[24] M. Bhukta, T. Dohi, V. K. Bharadwaj, R. Zarzuela, M.-A. Syskaki, M. Foerster, M. A. Niño, J. Sinova, R. Frömter, and M. Kläui, Nat. Commun. **15**, 1641 (2024).

[25] N. Kent, N. Reynolds, D. Raftrey, I. T. G. Campbell, S. Virasawmy, S. Dhuey, R. V. Chopdekar, A. Hierro-Rodriguez, A. Sorrentino, E. Pereiro, S. Ferrer, F. Hellman, P. Sutcliffe, and P. Fischer, Nat. Commun. **12**, 1562 (2021).

[26] D. Raftrey and P. Fischer, Phys. Rev. Lett. **127**, 257201 (2021).

[27] F. Zheng, N. S. Kiselev, F. N. Rybakov, L. Yang, W. Shi, S. Blügel, and R. E. Dunin-Borkowski, Nature **623**, 718 (2023).

[28] K. Ran, Y. Liu, Y. Guang, D. M. Burn, G. van der Laan, T. Hesjedal, H. Du, G. Yu, and S. Zhang, Phys. Rev. Lett. **126**, 017204 (2021).
[29] F. Zheng, F. N. Rybakov, A. B. Borisov, D. Song, S. Wang, Z.-A. Li, H. Du, N. S. Kiselev, J. Caron, A. Kovács, M. Tian, Y. Zhang, S. Blügel, and R. E. Dunin-Borkowski, Nat. Nanotechnol. **13**, 451 (2018).
[30] M. T. Birch, D. Cortes-Ortuno, K. Litzius, S. Wintz, F. Schulz, M. Weigand, A. Stefancic, D. A. Mayoh, G. Balakrishnan, P. D. Hatton, and G. Schutz, Nat. Commun. **13**, 3630 (2022).
[31] H. Jin, W. Tan, Y. Liu, K. Ran, R. Fan, Y. Shangguan, Y. Guang, G. van der Laan, T. Hesjedal, J. Wen, G. Yu, and S. Zhang, Nano Lett. **23**, 5164 (2023).
[32] P. W. Anderson, Science **177**, 393 (1972).
[33] B. Göbel, A. Mook, J. Henk, I. Mertig, and O. A. Tretiakov, Phys. Rev. B **99**, 060407(R) (2019).
[34] U. K. Rößler, A. N. Bogdanov, and C. Pfleiderer, Nature **442**, 797 (2006).
[35] H. Niu, H. Y. Kwon, T. Ma, Z. Cheng, C. Ophus, B. Miao, L. Sun, Y. Wu, K. Liu, S. S. P. Parkin, C. Won, A. K. Schmid, H. Ding, and G. Chen, Nat. Commun. **15**, 10199 (2024).
[36] K. Karube, L. Peng, J. Masell, X. Yu, F. Kagawa, Y. Tokura, and Y. Taguchi, Nat. Mater. **20**, 335 (2021).
[37] F. Zheng, N. S. Kiselev, L. Yang, V. M. Kuchkin, F. N. Rybakov, S. Blügel, and R. E. Dunin-Borkowski, Nat. Phys. **18**, 863 (2022).
[38] Z. He, Z. Li, Z. Chen, Z. Wang, J. Shen, S. Wang, C. Song, T. Zhao, J. Cai, S.-Z. Lin, Y. Zhang, and B. Shen, Nat. Mater. **23**, 1048 (2024).
[39] D. Yu, Y. Ga, P. Li, J. Jiang, J. Liang, L. Wang, C. Jia, K. Chang, and H. Yang, Phys. Rev. Lett. **133**, 206701 (2024).
[40] See Supplemental Material at [URL] for Section S1: method; Section S2: diverse symmetries of DM configurations and related magnetic textures; Section S3: structural and magnetic characterizations; Section S4: nonreciprocal spin-wave spectra; Section S5: MFM image and REXS characterization of the ground state magnetic order; Section S6: MFM analysis of the evolution of the magnetic textures; Section S7: micromagnetic simulations of magnetic structures; Section S8: large-area stabilization of bimeron lattice and the detailed phase diagram, which includes Refs. [41-46].
[41] C. Liu, S. Wu, J. Zhang, J. Chen, J. Ding, J. Ma, Y. Zhang, Y. Sun, S. Tu, H. Wang, P. Liu, C. Li, Y. Jiang, P. Gao, D. Yu, J. Xiao, R. Duine, M. Wu, C.-W. Nan, J. Zhang, and H. Yu, Nat. Nanotechnol. **14**, 691 (2019).
[42] I. Kézsmárki, S. Bordács, P. Milde, E. Neuber, L. M. Eng, J. S. White, H. M. Rønnow, C. D. Dewhurst, M. Mochizuki, K. Yanai, H. Nakamura, D. Ehlers, V. Tsurkan, and A. Loidl, Nat. Mater. **14**, 1116 (2015).
[43] M. Grelier, F. Godel, A. Vecchiola, S. Collin, K. Bouzehouane, A. Fert, V. Cros, and N. Reyren, Nat. Commun. **13**, 6843 (2022).
[44] X. Zhang, J. Xia, Y. Zhou, D. Wang, X. Liu, W. Zhao, and M. Ezawa, Phys. Rev. B **94**, 094420 (2016).
[45] A. O. Leonov and K. Inoue, Phys. Rev. B **98**, 054404 (2018).
[46] X. Zhang, Y. Zhou, X. Yu, and M. Mochizuki, Aggregate **5**, e590 (2024).
[47] Y. Zhang, J. Liu, Y. Dong, S. Wu, J. Zhang, J. Wang, J. Lu, A. Ruckriegel, H. Wang, R. Duine, H. Yu, Z. Luo, K. Shen, and J. Zhang, Phys. Rev. Lett. **127**, 117204 (2021).
[48] D. A. Kitchaev, I. J. Beyerlein, and A. Van der Ven, Phys. Rev. B **98**, 214414 (2018).

[49] S. Seki, Y. Okamura, K. Kondou, K. Shibata, M. Kubota, R. Takagi, F. Kagawa, M. Kawasaki, G. Tatara, Y. Otani, and Y. Tokura, Phys. Rev. B **93**, 235131 (2016).
[50] J. M. Lee, C. Jang, B.-C. Min, S.-W. Lee, K.-J. Lee, and J. Chang, Nano Lett. **16**, 62 (2016).
[51] J. Cho, N. H. Kim, S. Lee, J. S. Kim, R. Lavrijsen, A. Solignac, Y. Yin, D. S. Han, N. J. van Hoof, H. J. Swagten, B. Koopmans, and C. Y. You, Nat. Commun. **6**, 7635 (2015).
[52] H. T. Nembach, J. M. Shaw, M. Weiler, E. Jué, and T. J. Silva, Nat. Phys. **11**, 825 (2015).
[53] K. Zakeri, Y. Zhang, J. Prokop, T. H. Chuang, N. Sakr, W. X. Tang, and J. Kirschner, Phys. Rev. Lett. **104**, 137203 (2010).
[54] A. Prabhakar and D. D. Stancil, *Spin waves: Theory and applications* (Springer, 2009), Vol. 5.
[55] W. Legrand, D. Maccariello, F. Ajejas, S. Collin, A. Vecchiola, K. Bouzehouane, N. Reyren, V. Cros, and A. Fert, Nat. Mater. **19**, 34 (2019).
[56] C. Jin, Z.-A. Li, A. Kovács, J. Caron, F. Zheng, F. N. Rybakov, N. S. Kiselev, H. Du, S. Blügel, M. Tian, Y. Zhang, M. Farle, and R. E. Dunin-Borkowski, Nat. Commun. **8**, 15569 (2017).
[57] A. Vansteenkiste, J. Leliaert, M. Dvornik, M. Helsen, F. Garcia-Sanchez, and B. Van Waeyenberge, AIP Adv. **4**, 107133 (2014).
[58] W. Legrand, J. Y. Chauleau, D. Maccariello, N. Reyren, S. Collin, K. Bouzehouane, N. Jaouen, V. Cros, and A. Fert, Sci. Adv. **4**, eaat0415 (2018).

Figures

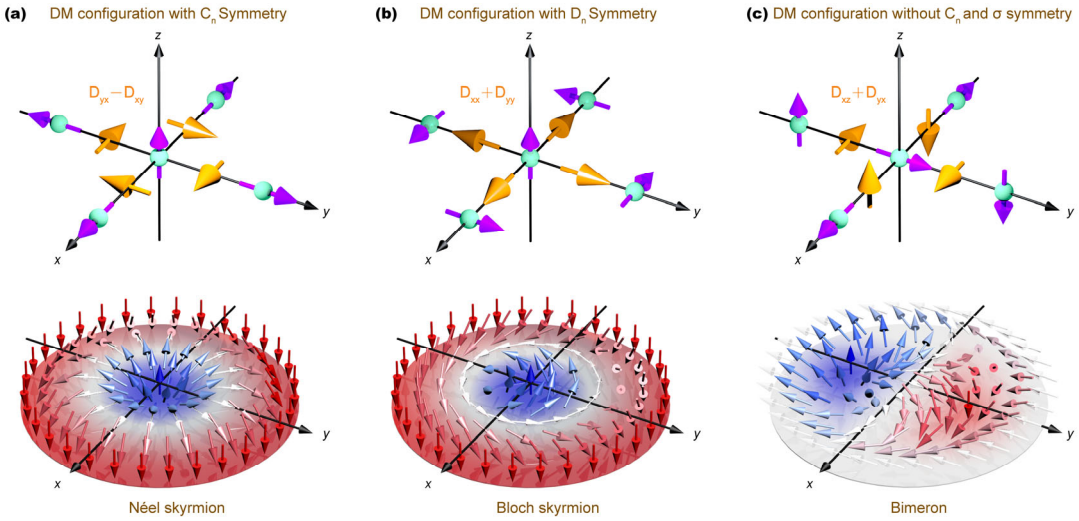

FIG. 1. DM configurations with different symmetries and corresponding energy-preferred topological spin textures. (a), (b) Classical DM configurations with rotational (C_n) or dihedral (D_n, combined C_n and mirror (σ) symmetry) symmetries and corresponding energetically stabilized Néel and Bloch-type skyrmions, respectively. **(c)** Three-dimensional DM configuration without C_n and σ symmetries and its associated bimeron state. Schematics of DM vector (orange arrows) distributions are shown in the top panels and the detailed magnetic textures are depicted in the bottom panels. The signs of the DM vectors are based on the relative orientation of neighboring ions/atoms (cyan balls).

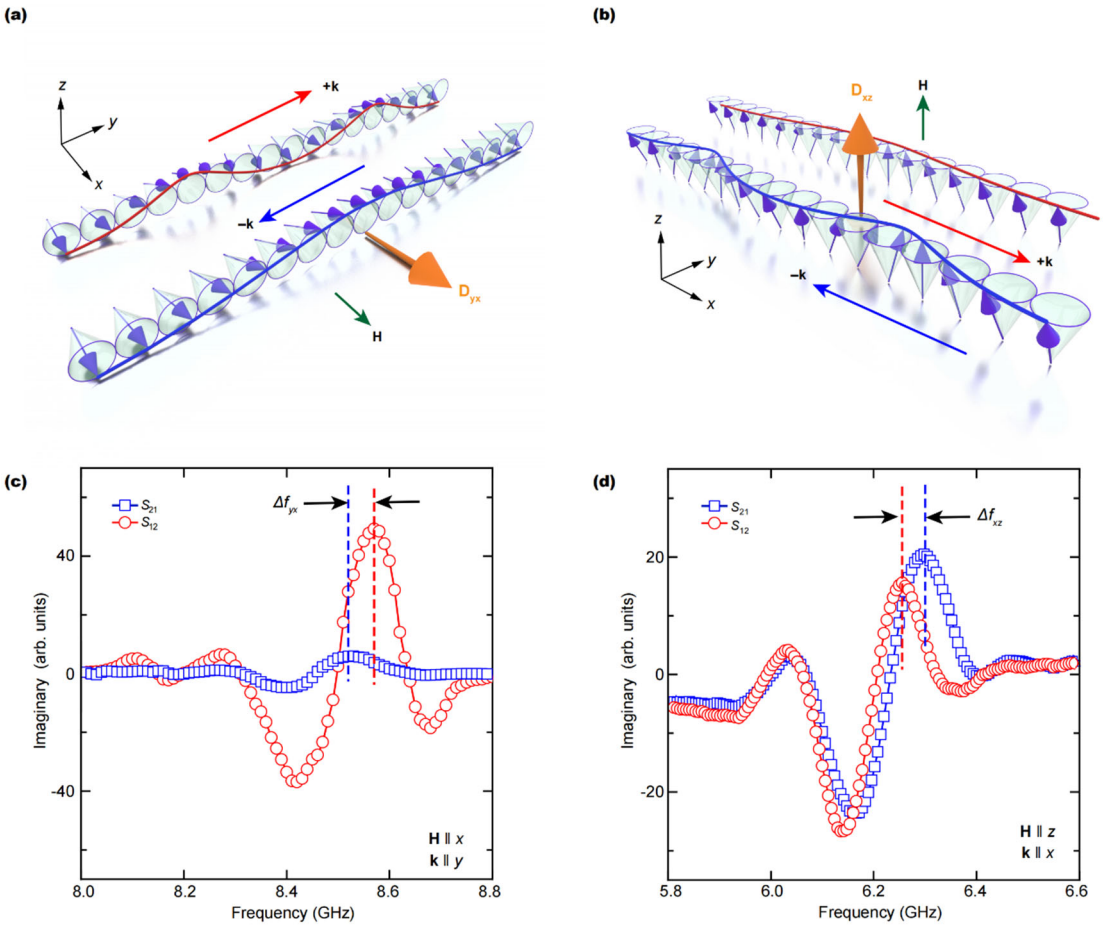

FIG. 2. Coexisting spin-wave frequency nonreciprocities induced by in-plane and out-of-plane DM components. (a), (b) Schematics of in-plane and out-of-plane DM vectors and their corresponding nonreciprocal spin-wave propagation, respectively. The DM component D_{yx} and D_{xz} are shown by orange arrows. The corresponding spin-wave vector $\pm\mathbf{k}$ (blue and red arrows) aligns along the y-axis (x-axis), and the external magnetic field $\mathbf{H}$ (green arrows) aligns along the x-axis (z-axis), respectively. **(c), (d)** Experimental transmission spectra of nonreciprocal spin-wave propagation at room temperature under $\mathbf{H} \parallel x$ and $\mathbf{H} \parallel z$ configurations, respectively. Spin waves in the transmission spectrum S_{21} $(+\mathbf{k})$ propagate from coplanar waveguide 1 (CPW1) to CPW2, while the S_{12} $(-\mathbf{k})$ spectrum describes propagation in the reverse direction.

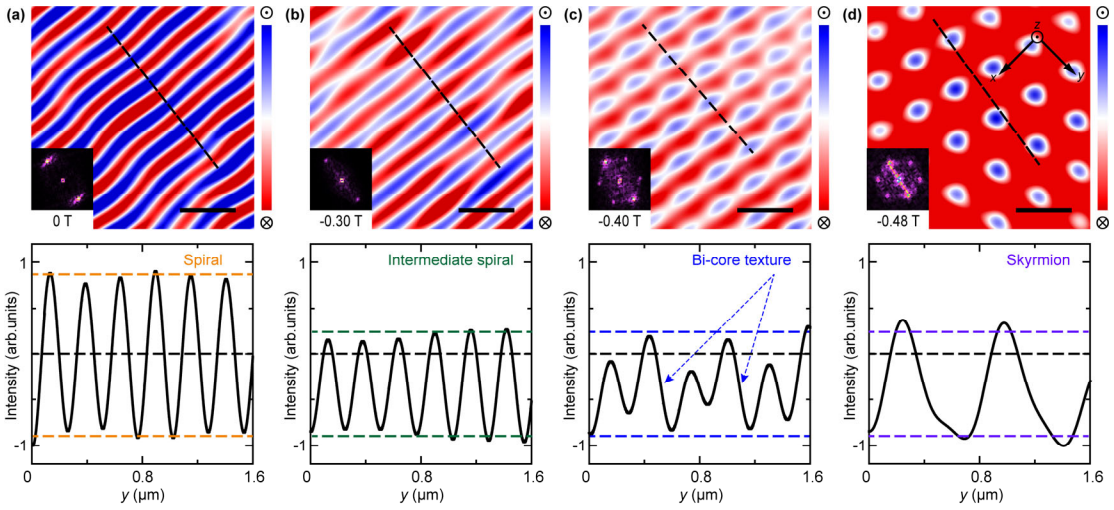

FIG. 3. Field-dependent evolution of spin textures. (a)-(d) Real-space images of spin textures under varying out-of-plane external fields (z-axis), captured by magnetic force microscopy (MFM) imaging (top panel). All scale bars represent 500 nm. The FFT patterns of different textures are displayed in the inset and illustrates their periodicities. The bottom panels show line plots along the y-axis, as indicated by the respective dashed lines above. The normalized stray field intensity from the local magnetization highlights the intensity differences between the spiral phase, intermediate spiral, bi-core lattice, and skyrmion phase.

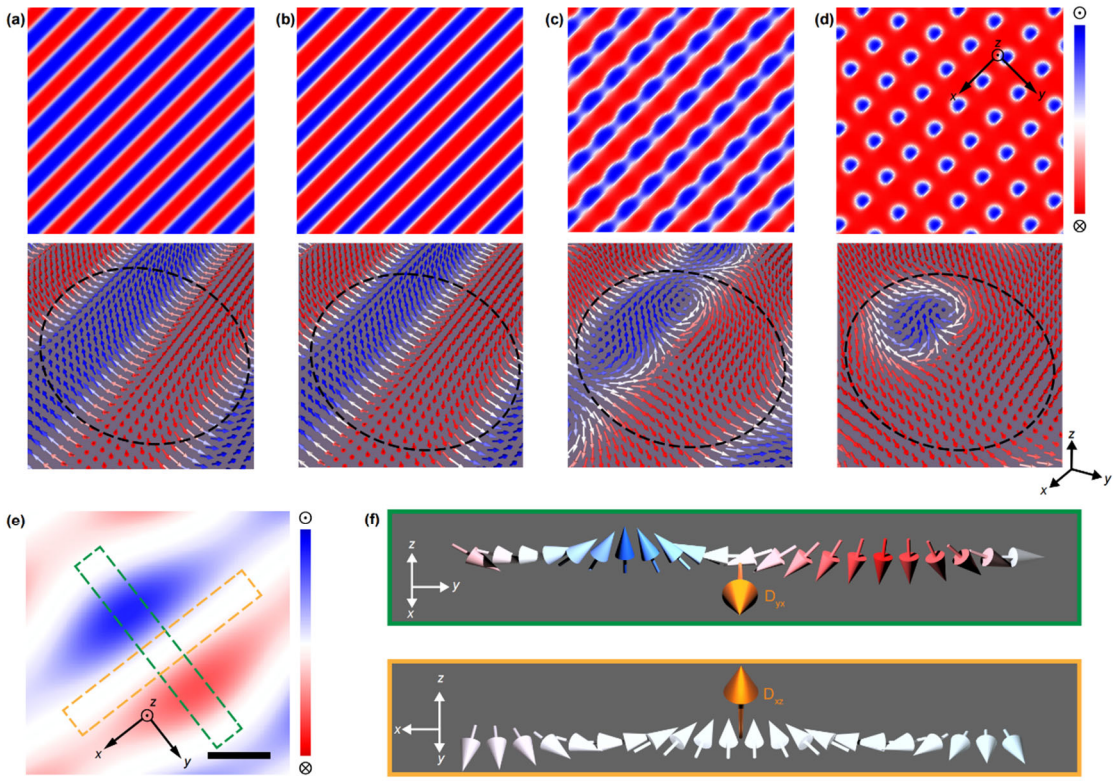

FIG. 4. The appearance of ferromagnetic bimeron lattice driven by in-plane and out-of-plane DM vectors. (a)-(d) Simulated results showing the progression from spiral to intermediate spiral, bimeron lattice, and finally skyrmion lattice. The corresponding top-layer spin configurations are depicted below each panel. Black circles indicate local transformations between textures across the sequence. **(e)** Experimentally observed bimeron unit cell. Yellow and green boxes highlight the distinct spin chiralities along the x- and y-directions, respectively. Scale bar: 250 nm. **(f)** Detailed comparison of spin chiralities within the bimeron structure: the green-boxed region (along y) displays out-of-plane chirality arising from the in-plane DM vector D_{xy}, while the yellow-boxed region (along x) shows in-plane chirality induced by the out-of-plane DM vector D_{xz}.